Supplementary Information

Biocompatible and structurally stable near-spherical PLNP@PDA@PW_{12} nanoplatforms for precise temperature sensing and photothermal therapy

Zhuwei Yang[a], Jian Yang[a,**], Xiaoyu Dong[a], Yangyang Zhao[b], Wanqin Yang[a], Bohan Lei[a], Lihua Zheng[c], Hancheng Zhu[a], Changshan Xu[a], Yongli Bao[c], and Yuxue Liu[a,*]

[a] *School of Physics, Northeast Normal University, 5268 Renmin Street, Changchun, 130024, China*

[b] *China-Japan Union Hospital of Jilin University, 126, Xiantai Street, Changchun, 130033, China*

[c] *National Engineering Laboratory for Druggable Gene and Protein Screening, Northeast Normal University, Changchun 130024, China*

**Corresponding author: yxliu@nenu.edu.cn (Yuxue Liu)*

***Corresponding author: yangj079@nenu.edu.cn (Jian Yang)*

1. Experimental Section

1.1. Characterization of the samples

XRD patterns of the samples were recorded using an X-ray diffraction spectrometer (D/MAX-2500, Rigaku) with Cu Kα radiation (λ = 1.5406 Å). Photoluminescence emission and excitation spectra were acquired using a Shimadzu RF-5301PC fluorescence spectrophotometer. For temperature-dependent emission measurements, an INSTEC HCS600 hot/cold stage was integrated with the spectrophotometer to precisely control sample temperature. Afterglow decay profiles were obtained using a Zolix Omicron-300 spectrofluorometer equipped with a pulsed xenon lamp. UV-Vis-NIR absorption spectra were

measured on a Shimadzu UV-3600 spectrophotometer with an integrating sphere attachment for enhanced accuracy. Morphological characterization was performed via scanning electron microscopy (SEM) using a FEI Quanta FEG 250 microscope and transmission electron microscopy (TEM) using a JEOL JEM-2100F microscope (JEOL, Japan) operated at 200 kV. FTIR spectra were collected on a Nicolet IS10 spectrometer (Thermo Fisher Scientific) in attenuated total reflectance (ATR) mode. Zeta potential values were determined using a Malvern Nano-ZS90 dynamic light scattering system. The biocompatibility of aqueous solutions of PLNP-PDA@PW_{12} nanoplatforms was evaluated by CCK-8 assay using a Microplate reader (Thermo, 354).

1.2 *In vitro* cytotoxicity and photothermal therapeutic evaluation

CCK-8 assay: L929 fibroblasts were cultured in complete DMEM medium supplemented with 10% fetal bovine serum (FBS) and 1% antibiotics, and maintained at 37°C in a humidified atmosphere containing 5% CO_2. Cells were seeded into 96-well plates at a density of 8,000-10,000 cells per well and allowed to adhere for 12 h. Following cell attachment, the culture medium was replaced with PBS solutions containing various concentrations (0, 12.5, 25, 50, 100, and 200 μg/mL) of PLNP-PB@PW_{12}, PLNP@PDA@PW_{12}, and ZGGO:Cr,Hf-Ag_2S nanoplatforms, and cells were exposed to these formulations for 24 h. Cell viability was subsequently evaluated using the CCK-8 assay by adding 10 μL of CCK-8 reagent per well and incubating for 1-4 h, followed by measurement of absorbance at 450 nm.

Photothermal therapy assessment: 4T1 breast cancer cells were cultured under identical conditions. After a 12-h incubation period following seeding, the cells were exposed to PLNP-PB dispersions at the same concentration range for 4 h. Subsequently, the cells were irradiated

with a 635 nm near-infrared (NIR) laser at a power density of 0.4 W/cm^2 for 5 min, followed by an additional 20-h incubation. Cell viability was then assessed as previously described.

1.3 Culture of pathogenic bacteria

Staphylococcus aureus and Escherichia coli lyophilized powders (purchased from Beijing Kezhang Biotechnology) were thawed at room temperature for 30 min under sterile conditions. Then we resuspended each strain in 3 mL of LB broth medium (25 g/L, autoclaved at 121 °C for 15 min) and transferred equal volumes of the bacterial suspensions into eight glass culture plates, each containing 12 mL of fresh LB medium. The plates were incubated in a shaking incubator at 65 rpm and 37 °C for 16-24 h. Bacterial cells were harvested by centrifugation (300 × g, 10 min per wash) and washed the pellets three times with PBST buffer. The cell pellets were resuspended in PBS buffer, and the culture-wash cycle was performed to ensure purity. Diluted 1 mL of the final suspension for immediate use. The remaining bacterial suspension in 20% sterile glycerol (2 mL per tube) was stored at -20 °C for long-term preservation.

2. The computational formulas

The following Equation S1 is used to describe the "Beer-Bouguer" formula [1]:

$$A = \varepsilon bc \tag{S1}$$

where A, ε, b, and c represent the absorbance, extinction coefficient, optical path length, and solution concentration of the sample, respectively.

The photothermal conversion efficiency of PB nanoparticles is given by Equation S2 [2]:

$$\eta = \frac{hA\left(\Delta T_{max,mix} - \Delta T_{max,H_2O}\right)}{\quad - A_{\lambda}} \tag{S2}$$

where h and A are the coefficients of heat transfer and surface area for the container,

respectively. $^{\Delta T_{max,mix}}$, and $^{\Delta T_{max,H_2O}}$ stand for the maximum temperature difference of PB nanoparticles aqueous solution and water when reaching thermal equilibrium under the surrounding environment, respectively. I is the laser power, and λ is the absorbance of the composite nanoplatforms at 635 nm.

Quantitative evaluation of afterglow stability using the reproducibility Equation S3 [3, 4]:

$$R = 1 - \frac{\max |\Delta C - \Delta i|}{\Delta C} \quad \text{(S3)}$$

where ΔC represents average afterglow intensity and Δi represents individual measurements.

3. Supplement figures

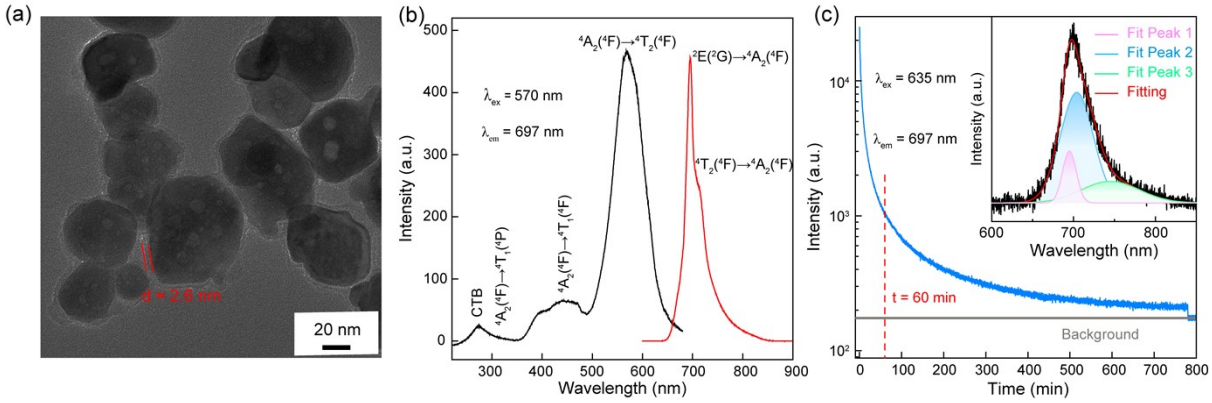

Figure S1. (a) TEM images of $Zn_2Ga_{2.96}Ge_{0.75}O_8:Cr^{3+}_{0.02},W^{6+}_{0.01}$@$SiO_2$-$NH_2$ nanoparticles (PLNPs). (b) Their excitation (λ_{em} = 697 nm) and emission (λ_{ex} = 569 nm) spectra. (c) Their afterglow decay curves were monitored at 697 nm after 5-min 635 nm irradiation. The inset shows the fitted phosphorescence spectrum.

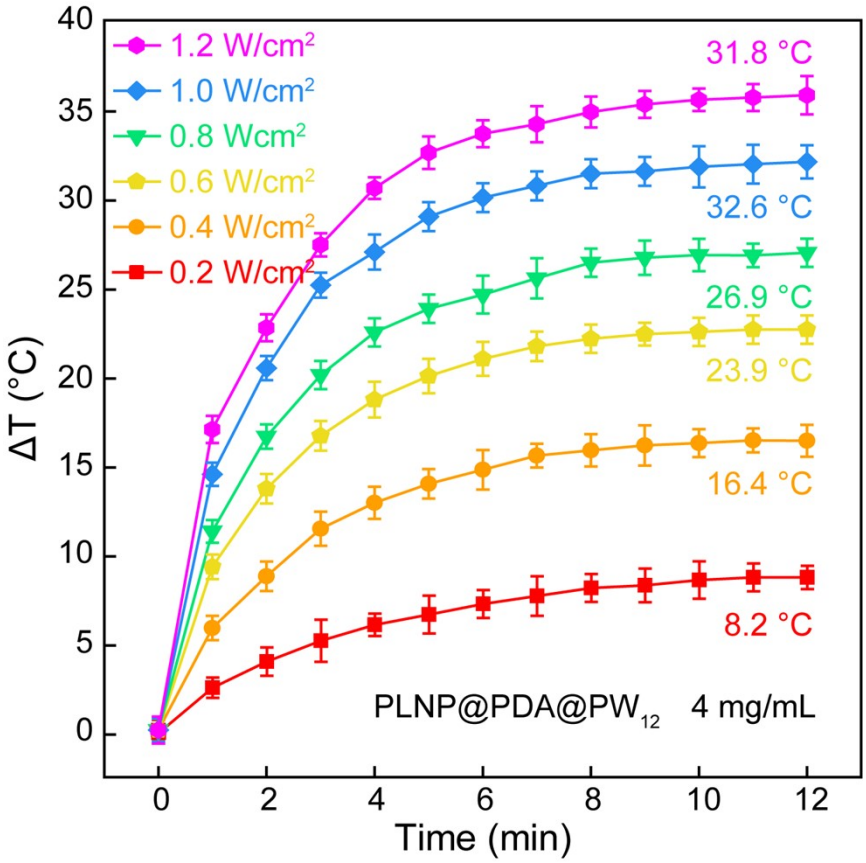

Figure S2. Temperature changes of 4 mg/mL PLNP@PDA@PW_{12} nanoplatforms aqueous solution under different 635 nm laser power densities.

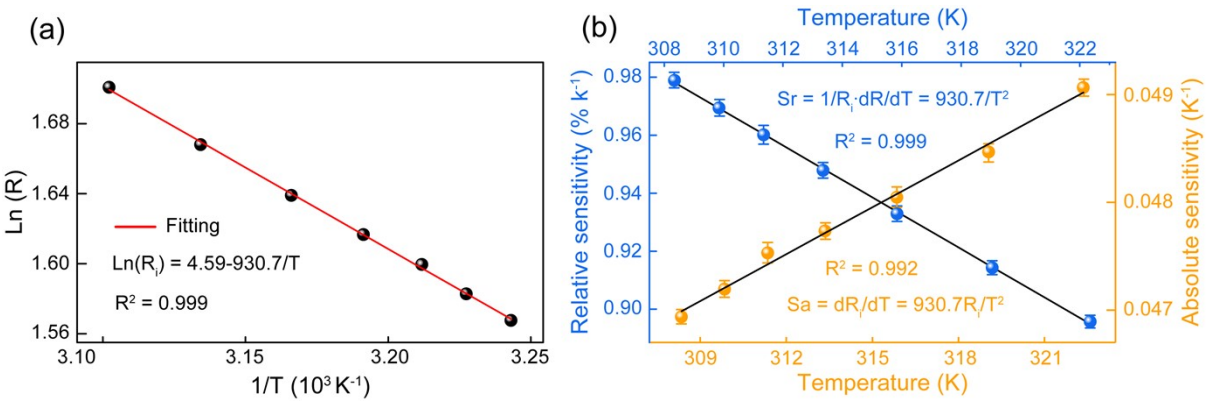

Figure S3. (a) Linear fitting curve of ln(R) versus 1/T. (b) The absolute and relative temperature sensitivities of the ratiometric afterglow nanothermometer based on Cr^{3+} ions occupying octahedral lattice sites.

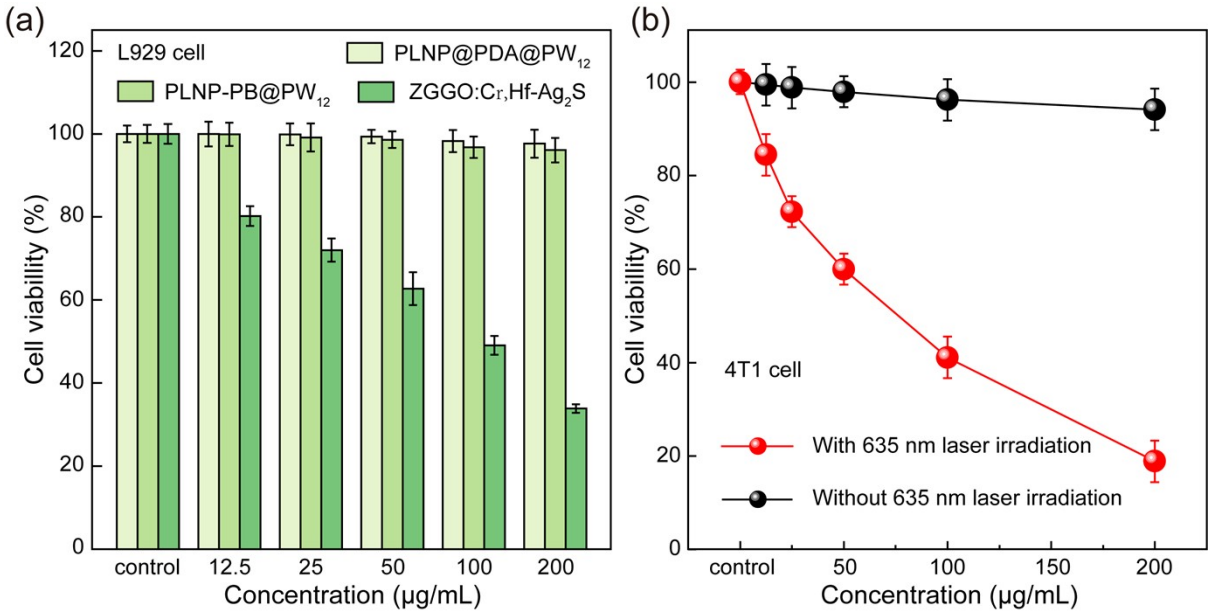

Figure S4. (a) Cell viabilities of L929 cells incubated with PLNP-PB@PW_{12}, PLNP@PDA@PW_{12}, and ZGGO:Cr,Hf-Ag_2S nanoplatforms PBS solutions at varying concentrations (0, 12.5, 25, 50, 100, 200 μg/mL) measured by CCK-8 assay. (b) The survival rates of 4T1 cells under 635 nm laser irradiation (0.4 W/cm^2, 10 min) and without irradiation using different concentrations of PLNP@PDA@PW_{12} nanoplatforms.

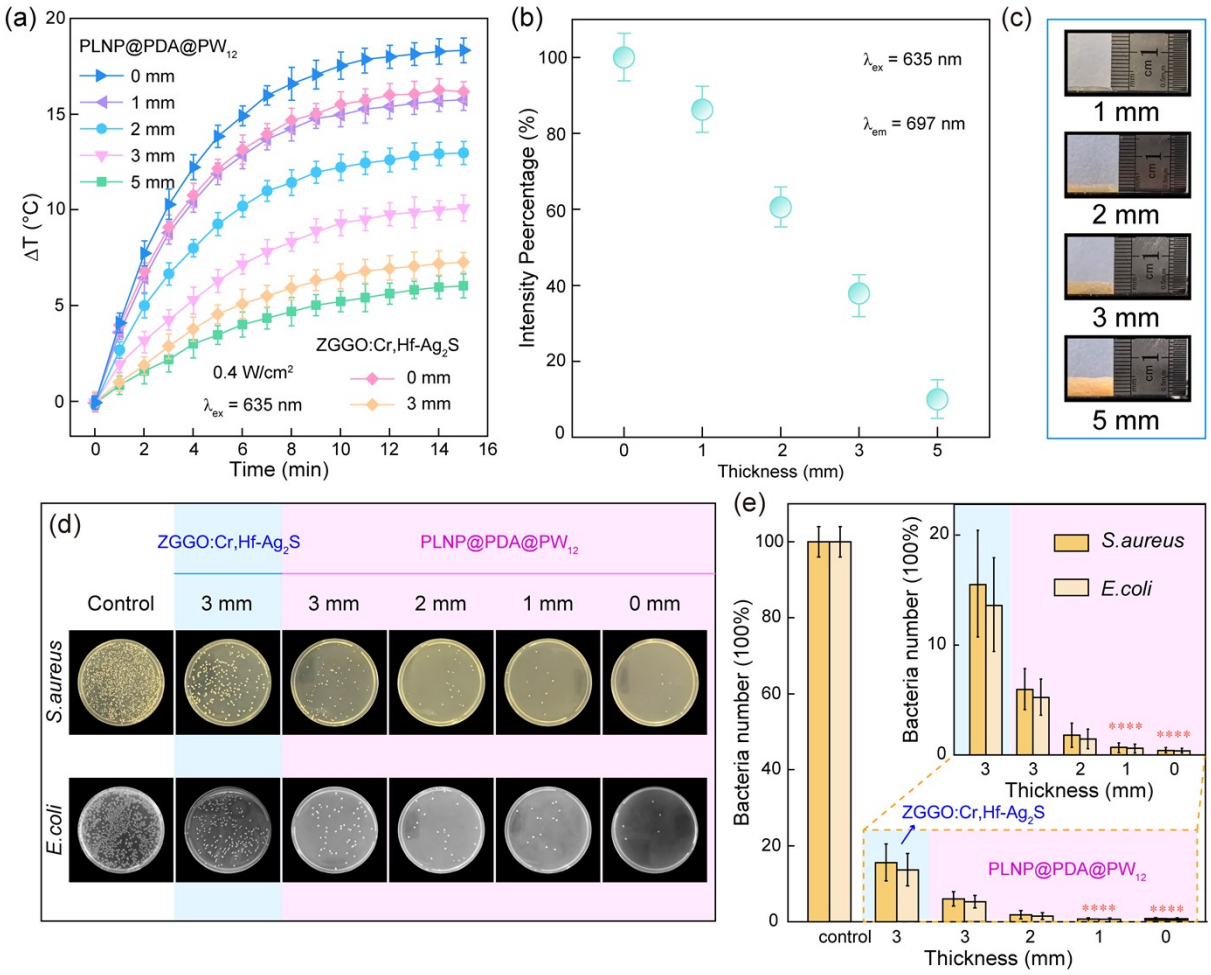

Figure S5. (a) The time-dependent temperature differences of 4 mg/mL PLNP@PDA@PW_{12} and ZGGO:Cr,Hf-Ag_2S nanoplatforms aqueous dispersion under the irradiation of a 635 nm laser (0.4 W/cm^2) that penetrates chicken tissues of varying thicknesses. (b) The normalized afterglow intensity of PLNP@PDA@PW_{12} nanoplatforms aqueous dispersion as a function of tissue thicknesses (1, 2, and 3 mm) after laser irradiation (635 nm, 0.6 W/cm^2, 15 min). (c) The images of chicken tissues with different thicknesses (1, 2, and 3 mm). (d) Colony growth plate photographs and (e) survival rates for *S. aureus*, *E. coli* PBS solution (1 mL) of PLNP@PDA@PW_{12} and ZGGO:Cr,Hf-Ag_2S nanoplatforms (10 μL, 4 mg/mL) PBS solutions through different chicken thicknesses (0, 1, 2, 3 mm) tissue under laser irradiation (635 nm, 0.4 W/cm^2, 10 min) after 24 h co-culturing. The inset of Fig.S5e shows a local magnified view. Significant differences between the two groups were noted by asterisks (*P < 0.05, **P < 0.01, ***P < 0.001,

****<0.0001). In panels (d) and (e), the photothermal antibacterial efficacy of ZGGO:Cr,Hf-Ag_2S nanoplatforms was evaluated under 3-mm-thick penetrating tissue.

Supplement references

1. X. Cai, X. Jia, W. Gao, K. Zhang, M. Ma, S. Wang, Y. Zheng, J. Shi and H. Chen, Advanced Functional Materials, 2015, 25, 2520-2529.
2. P. Huang, J. Lin, W. Li, P. Rong, Z. Wang, S. Wang, X. Wang, X. Sun, M. Aronova, G. Niu, R. D. Leapman, Z. Nie and X. Chen, Angewandte Chemie International Edition, 2013, 52, 13958-13964.
3. M. Back, E. Trave, J. Ueda and S. Tanabe, Chemistry of Materials, 2016, 28, 8347-8356.
4. Y. Li, J. Yang, M. Wang, Y. Zhu, H. Zhu, D. Yan, C. Liu, C. Xu and Y. Liu, Journal of Luminescence, 2022, 248, 118935.